Desalination and Water Treatment
www.deswater.com

doi: 10.1080/19443994.2015.1134353

57 (2016) 22413–22428
October

Taylor & Francis
Taylor & Francis Group

Biosorption of pulp and paper mill effluent by *Emericella nidulans*: isotherms, kinetics and mechanism

Anjali Singhal[a], Pawan Kumar Jha[a,b], Indu Shekhar Thakur[a,*]

[a]*School of Environmental Sciences, Jawaharlal Nehru University, New Delhi 110 067, India, emails: singhal.anjali@gmail.com (A. Singhal), pkjha@amity.edu (P.K. Jha), Tel. +91 11 26704321; +91 11 26191370; Fax: +91 11 26717586; email: indushekhart@gmail.com, isthakur@hotmail.com (I.S. Thakur)*
[b]*Amity Institute of Environmental Sciences, Amity University, Noida, Uttar Pradesh, India*

Received 8 April 2015; Accepted 11 December 2015

ABSTRACT

In this study, a fungus, *Emericella nidulans* (anamorph: *Aspergillus nidulans*), isolated from the sediments of a drain carrying effluent of pulp and paper mill, was used for biosorption of colour from pulp and paper mill effluent. The fungus turned dark brown in colour after treatment. Thus, its biosorption potential was studied in detail. The surface of the fungus was characterized by SEM and FT-IR analysis. The effect of change in pH, temperature, inoculum's size, contact time and initial concentration on colour adsorption was studied. The equilibrium data were studied using Freundlich, Langmuir, Elovich and Temkin equations. Best fitting model was Freundlich, used to describe heterogeneous systems. The pseudo-first-order and pseudo-second-order were used to fit adsorption data in the kinetic studies. The results showed that kinetics was best described by pseudo-second-order model. A detailed error analysis was undertaken. The mechanism of biosorption was governed by both external mass transport and intraparticle diffusion. The negative value of Gibbs energy change (ΔG°) indicates that the process was feasible and spontaneous. The value of activation energy (E_a) showed chemical adsorption, and positive value of isosteric heat of adsorption (ΔH_r) indicated that the process was endothermic. Adsorbents capable of removing pollutants from waste stream are widely applied in treating wastewater.

Keywords: Adsorption; Pulp and paper mill effluent; *Aspergillus nidulans*; Modelling; Instrumentation; Decolourization

1. Introduction

Pulp and paper industry is one among 17 major polluting industries in India. The effluent generated during pulping and bleaching is a complex mixture of hundreds of compounds like lignin, tannin, resin acids, fatty acids and their degraded products. These chemicals are responsible for the dark colour and toxicity of the effluent [1]. Treatment of effluent by adsorption on a synthetic or naturally occurring substance had been studied by many workers [2,3]. However, the use of micro-organism is usually limited to metal, phenolics and dye removal. In biosorption, either live or dead micro-organisms or their derivatives are used, which complex with chemicals through the action of ligands or functional groups located on the outer surface of the cell [4]. Micro-organisms

*Corresponding author.

including bacteria, algae, fungi and yeast are found to be capable of efficiently accumulating various chemicals/pollutants [5,6]. A number of fungi like *Penicillium*, *Aspergillus nidulans*, *Aspergillus niger*, etc. had been studied for biosorption [7–9]. The benefits of using fungus instead of physical adsorbents for treatment of pulp and paper mill effluent are that it can be composted. The lignin and its breakdown products will turn in to humus and then they can be used in fields as compost. Pulping stage effluent was used in this study as it was free from chlorinated compounds.

The phenomenon of biosorption is defined as a physiochemical process involving live entity like fungi or bacteria (adsorbent) and chemical or metal (adsorbate). Adsorbent i.e. fungi is in solid phase and adsorbate i.e. metal or chemicals is in liquid phase. Adsorption of pollutants is based on the partition process on a microbial biomass. This phenomenon is generally based on a set of chemical and physical mechanisms (involving physicochemical interactions such as electrostatic interactions, ion-exchange, complexation, chelation, precipitation, etc.) leading to the immobilization of a solute component on the microbial cell wall [10]. The complexity of the microbial structure implies that there are many ways for the pollutant to be captured by the cells. Cell walls of microbial biomass, mainly composed of polysaccharides, proteins and lipids, offer abundant functional groups, such as carboxyl, hydroxyl, phosphate and amino groups, as well as hydrophobic adsorption sites such as aliphatic carbon chains and aromatic rings [11]. This physicochemical phenomenon is quick and can be reversible.

Many studies have reported the use of fungi for biosorption especially in case of metals and dyes [12]. The study of biosorption involves detailed analysis of bioadsorbent, isotherm/kinetic studies and effect of pH, temperature, adsorbent dose, etc. Studies focusing on mycelium structure of fungi acting as an adsorbing medium through its polysaccharide components have been conducted [13,14]. The isotherm/kinetic studies help in explaining the process of biosorption. Different models are based on different assumptions. If a model fits process of adsorption then the assumptions becomes applicable for that particular adsorption process [15].

Biosorption is used in industries to treat wastewater. It is considered a low-cost, clean, efficient and simple to operate mechanism [12]. It is important to conduct kinetic and isotherm studies to understand the process of adsorption taking place at equilibrium. Complete characterization of adsorbent fungus with respect to wastewater is required before it can be applied commercially for bioremediation.

This work deals with detail analysis of the process of biosorption of pulp and paper mill effluent by *Emericella nidulans*. Previous study has shown that this fungus can remove coloured compounds present in pulp and paper mill effluent [16]. The fungal mycelium was characterized by SEM and Fourier transform infrared spectroscopy (FT-IR). Effect of variation in various parameters of biosorption was studied (temperature, pH, adsorbent dose, contact time and initial effluent concentration). Biosorption data were fitted into isotherms (Freundlich, Langmuir, Elovich and Temkin), kinetic models (pseudo-first-order and pseudo-second-order) and mechanism models (intra-particle diffusion and Boyd plot). Thermodynamic parameters ΔG, E_a and ΔH_r were calculated. All the studies were carried out in batch mode.

2. Material and methods

2.1. Preparation of adsorbate (effluent)

The adsorbate was MSM-effluent i.e. minimal salt media having in g/l: $Na_2HPO_4{\cdot}2H_2O$, 7.8; KH_2PO_4, 6.8; $MgSO_4$, 0.2; Fe $(CH_3COO)_3$ NH_4, 0.01; $Ca(NO_3)_2$ $4H_2O$, 0.05.This is the basic composition of MSM. It lacks carbon or nitrogen source. In this experiment, we have added varying amount of pulp and paper mill effluent as source of carbon and nitrogen. The effluent was collected from Anand tissue paper mill, UP [16].

2.2. Preparation of adsorbent (fungal biomass)

The fungi *E. nidulans* var. nidulans (anamorph: *A. nidulans*) having GenBank accession no: EU780786, deposited in Microbial Type culture collection, Chandigarh (MTCC no: 9654) was isolated previously from pulp and paper mill sediments [16]. It was grown in potato dextrose both (PDB) under shaking condition (125 rpm) and temperature (30°C). Spores were inoculated to obtain fungal mycelium in ball shape. Fungal mycelium balls (adsorbent) having diameter approximately 0.25 cm (5–6 d old culture) were used for adsorption studies. The fungal biomass was washed thoroughly with double distilled water to remove PDB.

2.3. Characterization of the fungal biomass

Changes in fungal biomass were studied before and after adsorption by scanning electron microscopy (SEM) and FT-IR.

2.3.1. SEM

The fungal mycelium before and after adsorption was fixed by soaking it overnight in 0.1 M phosphate buffer saline having 1% glutaraldehyde and 2% paraformaldehyde at 4°C. Fixed mycelium was smeared over the coverslip coated with poly-L-lysin for 30 min under wet condition. The specimen was washed with buffer, dehydrated in a series of ethanol–water solution (30, 50, 70 and 90% ethanol, 5 min each), and critical point dried under a CO_2 atmosphere for 20 min. Mounting on aluminium studs provided with adhesive disc, a line of silver paint was applied on two sides of each sample. A thin layer of gold was coated using Bio-rad Polaron Gold/Silver Sputter coating unit for 30 min. Coated cells were viewed at 15 kV with SEM (ZEISS Scanning Electron Microscope EVO 50). Working distance was 10 mm and SE1 detector was used. Rate of scanning and magnification varied with the sample.

2.3.2. FT-IR

The fungal mycelium before and after adsorption was washed, dried at 60°C to constant weight, ground and sieved through 4-mm sieve. The powder was then mixed with spectroscopy grade potassium bromide (KBr) in the ratio 1:99 w/w. Spectra were acquired in transmission mode. Scan was performed from 450 to 4,000 nm with Perkin-Elmer 1600 series FTIR Spectrometer (Nujol, KBr discs).

2.4. Effect of sorption parameters

The effect of varying pH (3–7); temperature (20–40°C); contact time (0–240 min); effluent concentration (2–17%) and fungal biomass (1–10%) was studied [17].

2.5. Adsorption (equilibrium) isotherms

Adsorption isotherms explain the interaction of adsorbate molecule (effluent) to the adsorbent (fungal biomass). For determination of adsorption isotherms accurately, weighed 3.75 g (7.5% w/v) fungal mycelium was added in MSM-effluent (50 ml) having carbon (dextrose, 0.25%), nitrogen (tryptone, 0.10%), rpm (125), temperature (30°C), inoculum size (7.5%), pH (5) and initial effluent concentration varying from 2 to 17%. On the basis of previous experiments (Section 3.2.4), it was observed that the equilibrium is established in 240 min. Hence, the contents of the flasks were analysed for residual colour concentration of MSM-effluent at 240 min. The various adsorption isotherms applied were Langmuir, Freundlich, Elovich and Temkin. The value of isotherm parameters was calculated and these parameters were used to calculate q_e non-linearly [15]. The details of isotherm equations are provided in Appendix A (Section A1).

2.6. Adsorption kinetics

For determination of adsorption kinetics, accurately weighed 3.75 g (7.5% w/v) fungal mycelium was added in MSM-effluent (50 ml) having carbon (dextrose, 0.25%), nitrogen (tryptone, 0.10%), rpm (125), temperature (30°C), inoculum size (7.5%), pH (5) and initial effluent concentration varying from 2 to 17%. The contents of the flasks were analysed for residual colour concentration of MSM-effluent at regular time intervals (30, 60, 120, 240 min). Kinetic models applied to the data were pseudo-first-order and pseudo-second-order. Various parameters were calculated and q_e was calculated using the value of these parameters linearly [17]. The details of kinetic models are provided in Appendix A (Section A2).

2.7. Error functions

The value of adsorption capacity (q_e^{calc}) was calculated non-linearly for isotherms and linearly for kinetic models. It was then compared with experimental values of q_e^{exp} to determine the error functions: coefficient of determination (r^2), average percentage error (APE), Chi-square (χ^2), sum of square (SSE), composite fractional error function (HYBRD), Marquardt's per cent standard deviation (MPSD), average relative error (ARE) and sum of the absolute errors (EABS) [15]. The details of equations for various error functions are provided in Appendix A (Section A3).

2.8. Mechanistic studies

2.8.1. Pore and film diffusion models

The most commonly used models to understand mechanism of biosorption are intraparticle diffusion plot (Weber–Morris plot) and Boyd plot [18,19]. Theoretical background of these models is given in Appendix A (Section A4).

2.8.2. Thermodynamics

Various thermodynamic parameters like activation energy (E_a) [20–22], Gibbs free energy (ΔG°) [2] and isosteric heat of adsorption (ΔH_r) [23] can be calculated using parameters obtained from isotherm/

kinetic models. The detail of these calculations is given in Appendix A (Section A5).

2.9. Analysis

The effluent samples were analysed for colour estimation by 2120C cobalt–platinate method [24]. Experiments were conducted in duplicate. Microsoft Excel 2007 was used for calculations and SigmaPlot 7 was used for making graphs and curve fitting.

2.10. Batch experiments

Most suitable value for each sorption parameter (pH 5; temperature 30˚C; fungal biomass 7.5% w/v; contact time 240 min) was chosen to conduct batch experiments. Initial effluent concentration varied from 2 to 17%. Batch experiments were conducted for determining adsorption isotherms, kinetics, thermodynamics and mechanism.

The amount of colour adsorbed by the fungal biomass was calculated using the following equation:

$$q_e = (C_o - C_e) \times V/W \quad (1)$$

where q_e is adsorbent capacity at equilibrium (mg/g). This is the amount of colour adsorbed by the fungus at equilibrium (Pt-Co U/g), C_o initial concentration of MSM-effluent (Pt-CoU/L), C_e concentration of MSM-effluent at equilibrium (Pt-Co U/L), V initial volume of MSM-effluent (ml), W weight of the adsorbent (g) [17]. The colour was measured in Platinum–Cobalt Unit (Pt-Co U) where 1 Pt-Co U is equivalent to one Hazen unit and to 1 mg/L of Platinum–Cobalt ion thus can be expressed as mg (Pt-Co)/L or simply mg/L [24]. Various parameters like colour, COD and TSS have been widely used for adsorption studies on effluent [2,3,25–27].

The per cent reduction in colour content of MSM-effluent was calculated using the following equation:

$$\text{Per cent reduction} = \left(C_o - C_t/C_o\right) \times 100 \quad (2)$$

where C_o is initial MSM-effluent concentration (mg/L), C_t MSM-effluent concentration at time t (mg/L).

3. Results and discussion

3.1. Characterization of fungal mycelium

3.1.1. SEM

SEM was used to observe changes induced by adsorption of effluent on fungal morphology. The surface of *E. nidulans* var. nidulans mycelia was studied at very high magnification. The SEM images of fungus before and after effluent adsorption are shown in Fig. 1(a) and (b). As shown in the SEM micrograph, the fungal mycelia have rough and porous surface. Porous surface provides increased surface area. In addition, these pores reduce the mass transfer resistance facilitating higher adsorption capacity and rate [28]. After adsorption, the deposition was clearly visible on the mycelium surface (Fig. 1(c) and (d)). Similar results have been observed in other studies [29,30].

3.1.2. FT-IR

FTIR spectroscopy allows identification of different functional groups present on the cell surface. Numerous chemical groups on the cell surface of fungal biomass, such as hydroxyl, amino and carboxyl groups are responsible for biosorption. Biosorption is dependent on factors such as quantity of sites, their accessibility, chemical state and affinity between site and effluent. The functional groups present on the cell surface can be identified by FTIR, as each group has a unique energy absorption band. The FTIR spectra of raw biomass of *E. nidulans* clearly demonstrate different functionalities present in the cell wall (Fig. 2(a)). The FT-IR analysis of the mycelium shows a broad band in the region 3,500–3,000 cm^{-1}. It is assigned to O–H and N–H stretching features of hydroxylic and primary amine and amide groups [21]. Peaks observed at 2,925.5 and 2,854.2 cm^{-1} represent asymmetric and symmetric deformation of $–CH_2$ groups, respectively. A peak at 1,646.7 cm^{-1} shows the bending of primary amines. The presence of these bands shows that the fungal mycelium was rich in chitosan and chitin. The peak observed at about 1,540 cm^{-1} represents N–H stretching of the primary and secondary amides [31]. The phosphate group presents certain characteristic absorption peaks (P=O stretching at 1,150 cm^{-1}; P–OH stretching at 1,100–1,030 cm^{-1}; P–O–C stretching at 1,050–970 cm^{-1}).

Therefore, the peaks observed at 1,154, 1,080 and 1,030 cm^{-1} indicated the presence of the phosphate functional groups [31–33]. The band between 610 and 535 cm^{-1} for the fungal preparations represents C–N–C scissoring and are found in protein structure [21]. The functional groups important for biosorption (carboxyl, amino and phosphate) were identified in the fungal biomass (Fig. 2(a)). The effluent from pulp and paper mill has degradation products of lignin, hemicellulose and cellulose. FT-IR spectra of dried effluent sample showed characteristic bands for lignin/hemicellulose at 3,390.1, 1,574.4, 1,258.9, 1,210.4 and 837.4 cm^{-1} (Fig. 2(b)) [34]. On analysing the mycelium with effluent adsorbed onto it (Fig. 2(c)), the peak characteristic

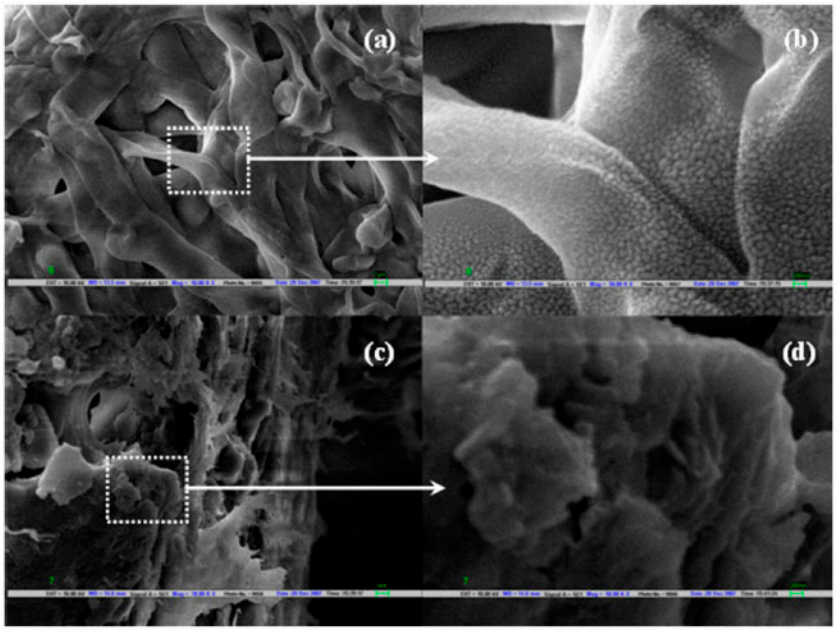

Fig. 1. SEM of *E. nidulans* (a) before biosorption at 10,000 magnification, (b) before biosorption at 50,000 magnification, (c) after biosorption at 10,000 magnification and (d) after biosorption at 50,000 magnification.

of fungal mycelium (3,450, 2,925.5, 1,746.9, 1,646.7 and 1,157.4 cm^{-1}) as well as peaks of lignin/hemicellulose (1,258.9, 1,210.4 and 837.4 cm^{-1}) were present.

3.2. Effects of different factors on adsorption process

3.2.1. Effect of temperature

The temperature of biosorption medium could be important for energy-dependent mechanism in biosorption by microbial biomass. The effect of temperature on equilibrium biosorption capacity q_e and per cent reduction in colour content of effluent was studied in the range 20–40˚C (Fig. 3(a)). The biosorption of effluent increased with increasing temperature from 20 to 30˚C. Apart from the apparent endothermic nature, the adsorption mechanism may be controlled by diffusion, as the adsorbent is porous in nature. The increase in temperature favours effluent transport within the pores of the fungal mycelium. The increase in adsorption with temperature may also be attributed to the increase in the number of adsorption sites generated due to breaking of some initial bonds near the edge of the active surface site of the adsorbent [17]. In most of the studies suitable temperature was in the range 30–35˚C [21,28,35].

3.2.2. Effect of pH

The biosorption is highly dependent on the pH of a solution. The solution's pH affects the chemistry of the chemicals present in effluent, the activity of functional groups (carboxylate, phosphate and amino groups) on the cell wall, as well as the competition of various compounds for the binding sites. Complex organic compounds having different aromatic rings and functional groups have different ionization potentials at different pH and therefore their interaction with microbial biomass depends on the chemistry of a particular compound and the specific chemistry of the biosorbents. Different functional groups become active at different pH, which favours the absorption process [36]. From the study, it can be seen that effluent biosorption increased with a rise in pH (Fig. 3(b)). q_e as well as per cent reduction in colour content of effluent was highest at pH 5, i.e. 419 mg g^{-1} and 24% removal. *Corynebacterium glutamicum* biomass was used for biosorption of synthetic dye effluent at pH 5 [37]. Literatures have reported a wide range of optimum pH from highly acidic conditions to slightly alkaline conditions. Highly alkaline conditions are usually not suitable for biosorption [38].

3.2.3. Effect of adsorbent dosage

A range of biomass dosage from 1, 2.5, 5, 7.5 and 10% (w/v) was used to obtain the maximum amount of effluent biosorption by *E. nidulans*. Adsorption capacity decreased with increasing biomass dosage from 645 to 368 mg/g, while per cent colour removal

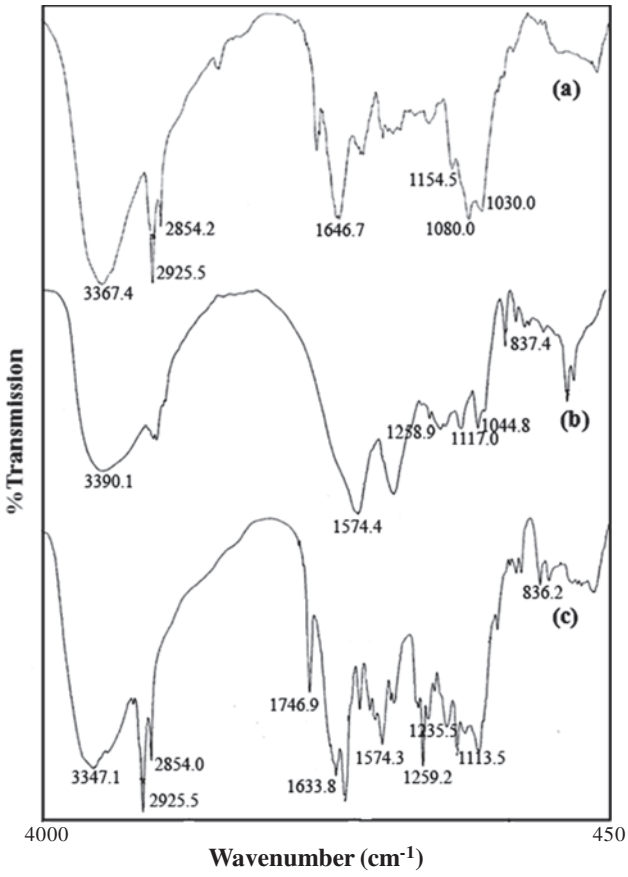

Fig. 2. FT-IR spectra of (a) unadsorbed *E. nidulans*, (b) dried effluent and (c) effluent adsorbed *E. nidulans*.

increased from 7 to 25% (Fig. 3(c)). Similar trend was observed in another study using neem leaves for chromium ion, Cr(VI) adsorption. There was drop of 14.9 to 3.74 mg/g in q_e, while per cent removal increased from 99.5 to 99.9% [39]. Correlation analysis was done in between adsorbent dosage vs. per cent removal and adsorbent dosage vs. q_e. There was significant positive correlation (+0.94) in between adsorbent dosage vs. per cent removal and negative correlation (–0.96) in between adsorbent dosage vs. q_e. The increase in colour removal may be due to the increase in amount of free surface available [17]. The decrease in adsorbent capacity was due to decrease in number of effluent ions available per unit mass of adsorbent [39]. Most suitable adsorbent dosage was 7.5% (w/v). Rests of the experiments were carried out at this dose.

3.2.4. Effect of contact time

Experiments were conducted at different durations (contact time) to find out equilibrium end point. Duration was varied from 0 to 300 min. From the experimental data, it was observed that percentage adsorption increased with increasing contact time up to 240 min and stabilized after that (Fig. 3(d)). There was significant positive correlation in between increasing contact time and per cent removal (+0.90) as well as with q_e (+0.88). It was observed that initially the adsorption rate was fast, followed by slower rate. The mechanism of adsorbate transfer to the solid includes diffusion through the fluid film around the adsorbent and diffusion through the pores to the internal adsorption sites. Initially the concentration gradient between the liquid phase and the solid surface was large, and hence the transfer of solute onto the solid surface was faster. As time increases, intraparticle diffusion becomes predominant. Hence, solute takes more time to transfer from solid surface to internal adsorption sites through the pores [39]. Equilibrium was reached in 240 min, hence rest of the experiments were carried out for 240 min. The time required to reach equilibrium state varies with adsorbent, adsorbate and process conditions. Durations as short as few minutes have been reported. Contact time of 60 min was required to reach equilibrium for hexavalent chromium biosorption on *A. junii* [40]. Equilibrium time for biosorption of Reactive blue 4 by *P. chrysosporium* was 240 min [21]. In our study also suitable contact time was 240 min. Duration as long as 720 and 1,440 min had been reported for biosorption of pentachlorophenol and phenol, respectively [33,41].

3.2.5. Effect of initial effluent concentration

The effect of initial effluent concentration on biosorption was studied by varying the initial effluent concentration from 2 to 17% while maintaining the fungal biomass at 7.5% w/v. It was observed that per cent colour removal decreased from 35 to 21% and adsorbent capacity q_e increased from 97.6 to 586.9 mg/g with increasing initial effluent concentration C_o (Fig. 3(e)). Significant negative correlation was found in between increasing effluent concentration and % removal (–0.93). However, the change had positive influence on q_e and correlation coefficient was +0.99. Decrease in percentage removal of colour may be due to an increase in the number of effluent molecules for the fixed amount of adsorbent. The amount of colour adsorbed per unit mass of *E. nidulans* increased may be due to the complete utilization of adsorption surface and active sites available which was not possible in low effluent concentration. Similar variations were observed when neem leaves were used to adsorb chromium ion, Cr(VI) in the range 40–700 mg/l. The per cent metal ion removal decreased by 10% and q_e increased from 3.98 to 62.9 mg/g [39].

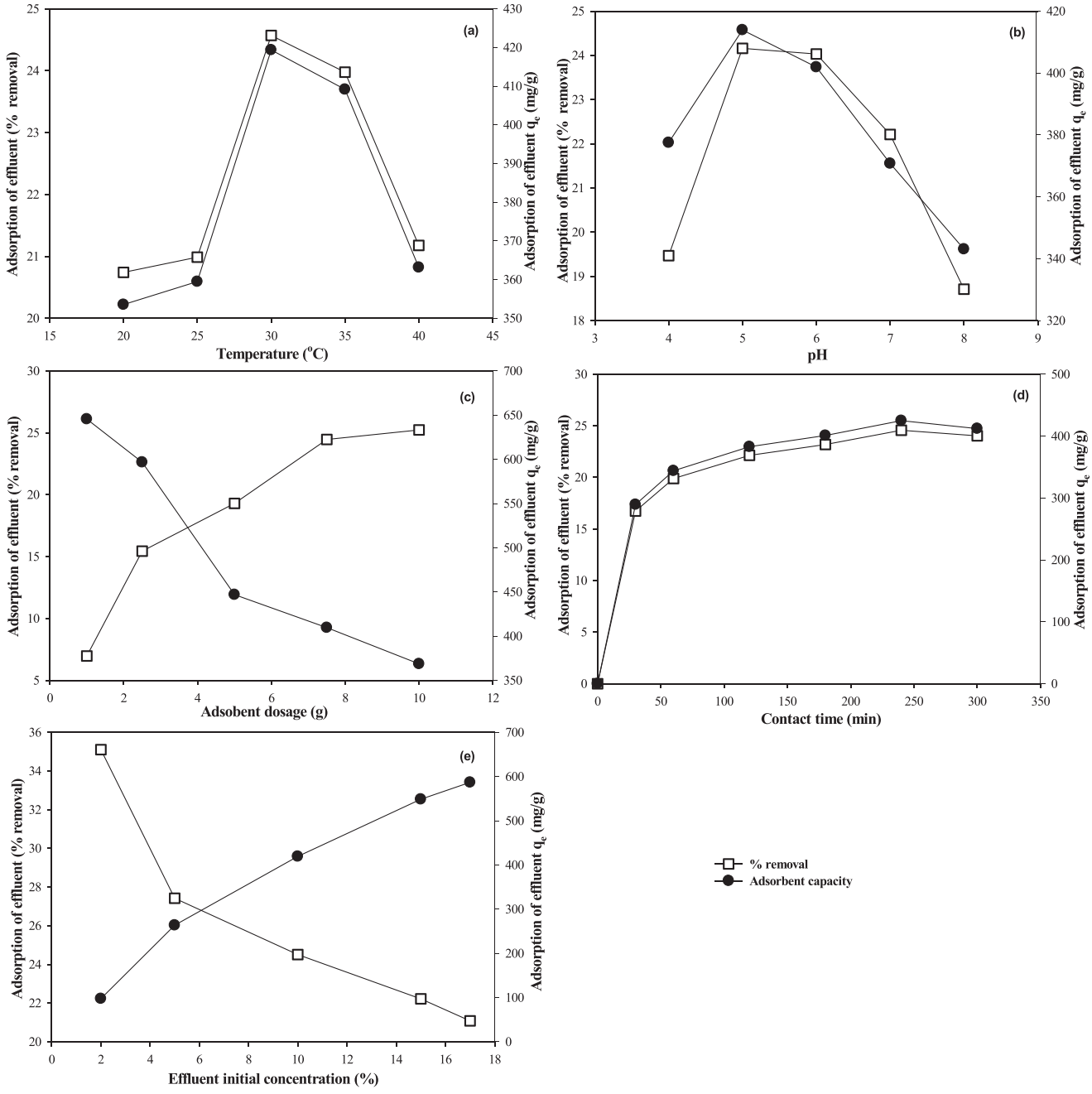

Fig. 3. Effect of variation of (a) temperature, 20–40˚C, (b) pH, 4–8, (c) adsorbent dose, (1–10%), (d) contact time, 30–300 min and (e) initial effluent concentration, 2–17% on biosorption capacity of *E. nidulans*.

3.3. Adsorption isotherms

In this study, estimation of colour was used as criteria for effluent adsorption. Effluent was a complex mix of large number of chemicals. It was not feasible to study each of them individually hence colour was taken as an indication for chemicals present in the effluent [42]. Among the four isotherm models tested, Freundlich isotherm fits best to the experimental equilibrium data with r^2 value 0.999 followed by Langmuir 0.997, then Elovich 0.966 and finally Temkin at 0.952. Freundlich isotherm is one of the most widely used empirical expressions that accounts for the surface heterogeneity, exponential distribution of active sites of sorbent and their energies toward adsorbate. The model

assumes that as the adsorbate concentration increases, the concentration of adsorbate on the adsorbent surface also increases [3]. Similar results were observed when effluent concentration was increased from 2 to 17% (Fig. 1(e)). The value of n was 1.38, which lies within 1–10 indicated favourable adsorption and heterogeneous nature of fungal mycelium [28]. The value of Freundlich constant K_f was 0.872 (mg/g)(L/mg)$^{1/n}$. The predicted q_e using Freundlich parameters was:

$$q_e = 0.872\, C_e^{0.7251} \tag{3}$$

Langmuir isotherm slightly diverges with experimental results for higher equilibrium concentration (Fig. 4). The value of Langmuir constant K_L was 0.000176 L mg^{-1} and q_m was 909.0909 mg/g. R_L a dimensionless equilibrium parameter was calculated using Langmuir constant K_L and initial effluent concentration C_o. The value of R_L for 2% effluent concentration was 0.84, for 5% was 0.61, for 10% was 0.47, for 15% was 0.38 and for 17% was 0.35. All the values lie in the range 0–1 indicating favourable process. However, the value of R_L was decreasing with increasing effluent concentration. Similar results were observed when fly ash was used for sorption of distillery effluent [3]. The predicted q_e using Langmuir parameters was:

$$q_e = (909.09 \times 0.000176 \times C_e)/(1 + 0.000176 \times C_e) \tag{4}$$

Freundlich and Langmuir mode of adsorption had been reported in many fungi used for biosorption of effluent by *A. niger* [43], *L. sajor-caju* [28], *P. chrysosporium* [21], *E. nidulans* [44] etc.

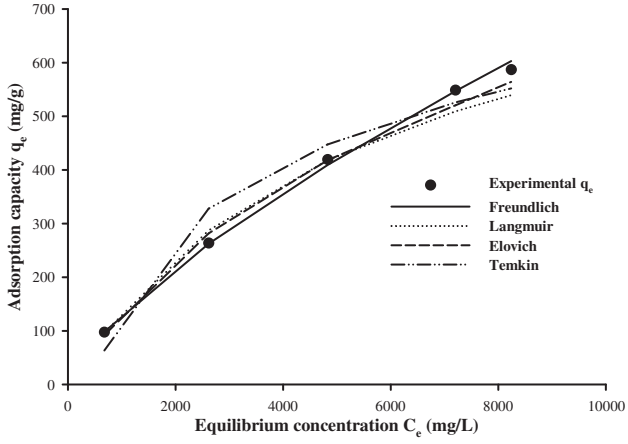

Fig. 4. Comparison of experimental equilibrium data (points) and Freundlich, Langmuir, Elovich and Temkin isotherms (curves) for biosorption of effluent onto *E. nidulans*.

Langmuir, Elovich and Temkin isotherm models, despite having high r^2 value, were less suitable than Freundlich isotherm (Fig. 4 and Figs. B1–B4). Fitness of isotherm models were evaluated using various error functions i.e. r^2, APE, χ^2, SSE, HYBRD, MPSD, ARE and EABS. The values for error functions is given in Table 1 [15,45]. According to error functions Elovich was a better fitting model as compared with Langmuir. Freundlich was the best fitted model (Table 1). The value of Elovich parameters K_E was 0.000218 L mg^{-1} and q_m was 714.28 mg/g. The predicted q_e using Elovich parameters was:

$$q_e/714.2857 = 0.000218 \times C_e \,\mathrm{Exp}\left(-q_e/714.2857\right) \tag{5}$$

The value of Temkin parameter (RT/ΔQ) was 0.002044 and K_T was 195.44 L mg^{-1}. The predicted q_e using Temkin parameters was:

$$q_e = 195.44\, \ln(0.002044313 C_e) \tag{6}$$

Low r^2 value of Temkin isotherm confirms that fungal surface was heterogeneous.

3.4. Kinetic model

The relationship between contact time and effluent uptake by *E. nidulans* was studied through batch kinetic experiments that were carried out at five different initial concentrations ranging from 2 to 17% effluent at predetermined adsorbent mass (Fig. 5) The kinetics of sorption describes the solute uptake rate, which in turn governs residence time or sorption reaction. It is one of the important characteristics in defining the efficiency of biosorption [46]. In the present study, kinetics of colour removal was carried to understand the process of decolourization of pulp and paper mill effluent by *E. nidulans*. The experimental kinetic data of biosorption studies was applied to pseudo-first-order and pseudo-second-order.

The coefficient of determination (r^2) values for pseudo-second-order (Table 2) shows that it was better fitting model than pseudo-first-order kinetic model. Second-order kinetics is thought to drive from biosorption process in which the rate-controlling step is an exchange reaction. The calculated q_e values from the pseudo-second-order are in good agreement with the experimental q_e values (Fig. 5). Pseudo-second-order plot t/q_t vs. t was linear (supplementary data), thus adsorption was chemisorption [47]. The rate constant calculated for pseudo-first-order and pseudo-second-order is given in Table 2 (Appendix A Figs. B5

Table 1
Value of different Error functions calculated for experimental (q_e^{exp}) and calculated (q_e^{calc}) adsorption capacity for various isotherm and kinetic models. (Most suitable model for both isotherm and kinetics is highlighted as bold)

	APE (%)	χ^2	SSE	HYBRID	MPSD	ARE	EABS
Isotherms							
Freundlich	**1.360**	**0.693**	**361.899**	**0.697**	**0.001**	**0.068**	**30.107**
Langmuir	5.050	9.280	4,422.573	8.881	0.020	0.252	112.766
Elovich	4.427	4.002	1,692.274	3.945	0.012	0.221	76.471
Temkin	15.254	36.037	7,833.075	32.546	0.192	0.763	184.567
Kinetics							
Pseudo-first-order	52.80	2,010.573	366288.7	720.295	1.529	2.640	1,156.635
Pseudo-second-order	**8.856**	**11.031**	**4,909.624**	**11.970**	**0.043**	**0.443**	**148.236**

and B6). The error functions are given in Table 1. The initial adsorption rate (Ho constant), h_o calculated from the curve of pseudo-second-order increased with increasing effluent concentration (Table 2) shows that rate of adsorption was faster for higher effluent concentration [20].

3.5. Adsorption mechanism

3.5.1. Pore and film diffusion models

Kinetic and equilibrium studies help to identify the sorption process, predicting the mechanism required for design purpose. The external mass transfer (boundary layer effect) or intraparticle diffusion or both can characterize the biosorption process. The following three steps can describe the sorption dynamics:

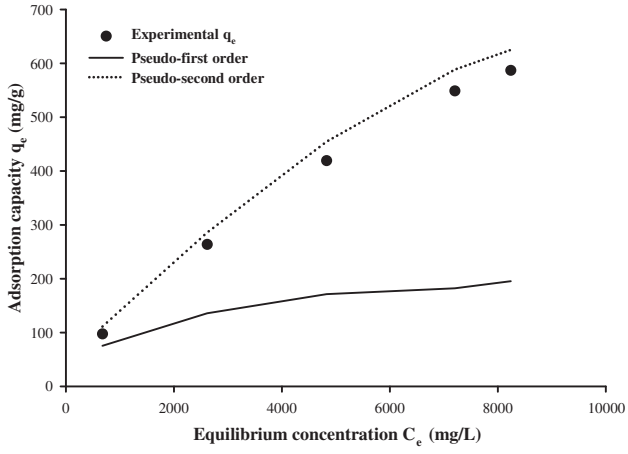

Fig. 5. Comparison of experimental kinetic data (points) and Pseudo-first-order and Pseudo-second-order (curves) for biosorption of effluent onto *E. nidulans*.

(1) Transfer of solute from bulk solution through liquid film to the adsorbent exterior surface (film diffusion).
(2) Solute diffusion into the pore of adsorbent except for a small quantity of sorptionon the external surface; parallel to this is intraparticle transport mechanism of the surface diffusion (pore diffusion).
(3) Sorption of the solute on the interior surface of the pores and capillary spaces of adsorbent [3,48].

Of the three steps, third step is assumed to be rapid and negligible. The most commonly used technique for identifying the mechanism involved in the biosorption is by fitting the experimental data to intraparticle diffusion plot i.e. Weber–Morris plot. A plot was made in between q_t vs. $t^{0.5}$ (Fig. 6). The sorption process tend to follow two phases, initial sharper portion indicating boundary layer effect (also called film diffusion or external mass transfer) and second linear portion indicating intraparticle or pore diffusion (Fig. 6). According to the intraparticle diffusion model, a linear plot passing through origin indicates that the rate is controlled by intraparticle diffusion. Intercept of the plot reflects boundary layer effect (also called external mass transfer) and it was increasing with increasing effluent concentration (Table 2) [48]. Similar results were observed when fly ash was used for biosorption of colour from distillery effluent [3]. The value of intraparticle diffusion constant Ki was also increasing with increasing effluent concentration (Table 2). This can be explained by the growing effect of driving force, the effluent concentration gradient [18]. The Weber–Morris plots were linear (r^2 ranged from 0.95 to 0.98; Table 2) but did not pass through origin. This indicates that mechanism of colour

Table 2
Kinetic constant for pulp and paper mill effluent adsorption on *E. Nidulans*

	First-order-model			Second-order-model				Weber–Morris model		
Effluent concentration (%)	r^2	q_e (mg/g)	k_f (min^{-1})	r^2	q_e (mg/g)	k_s (g/mg min)	h_o (mg/g min)	r^2	k_i (mg/mg $min^{0.5}$)	I
2	0.926	75.331	0.0344	0.992	111.111	0.0002	2.984	0.985	4.2821	33.206
5	0.979	135.775	0.030	0.996	285.70	0.00014	12.019	0.964	8.6862	132.89
10	0.987	171.263	0.026	0.998	454.54	0.00011	23.310	0.958	12.604	229.81
15	0.945	182.05	0.0211	0.995	588.235	0.00009	33.445	0.979	12.687	346.44
17	0.932	195.31	0.0233	0.995	625.00	0.0009	38.023	0.976	13.081	380.29

removal by *E. nidulans* was complex and both the mass transfer as well as intraparticle diffusion contributes to the rate-determining step [49].

In order to predict the actual slow step involved, the kinetic data were further analysed using the Boyd kinetic expression. Plots were drawn for various effluent concentrations in the range 2–17% (Fig. 7). The plots were linear but do not pass through origin, it shows that mass transfer was the main controlling factor at initial stage followed by intraparticle diffusion at later stage [19].

3.5.2. Thermodynamics

The nature of biosorption varies with the micro-organism used, process parameters and contaminant adsorbed. It can be endothermic as well as exothermic. The process can be physical or chemical [10,50].

3.5.2.1. Gibbs free energy (ΔG°). The Gibbs free energy of adsorption (ΔG°) was calculated using Langmuir constant. Its value at 30°C was −32.72 kJ/mol. Negative value of ΔG° indicated that the process was feasible and spontaneous [51].

3.5.2.2. Isosteric heat of adsorption (ΔH_r). The value of ΔH_r calculated for the temperature range 303–318 K was found to be 2.16 kJ mol^{-1}. The positive value of heat of adsorption (ΔH_r) indicated that the process was endothermic in nature [23].

3.5.2.3. Activation energy (E_a). The parameters calculated from pseudo-second-order model were used to calculate activation energy E_a. The magnitude of E_a may give idea about the type of adsorption (i.e. physical or chemical). In physical adsorption equilibrium is attained rapidly and E_a is usually lesser than 4.2 kJ/mol [21]. On the other hand, chemical sorption is specific and involves force much stronger than in physical sorption. The magnitude of E_a varied from 24.528 to 33.521 kJ/mol for different initial effluent concentrations. Thus, the chemical sorption was taking place.

Results indicate that the process of adsorption of effluent by *A. nidulans* was spontaneous. Previous

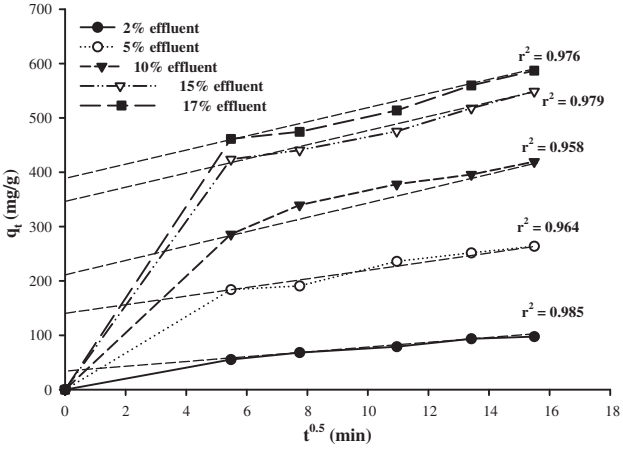

Fig. 6. Intraparticle diffusion plots for effluent adsorption onto *E. nidulans* at different effluent concentrations.

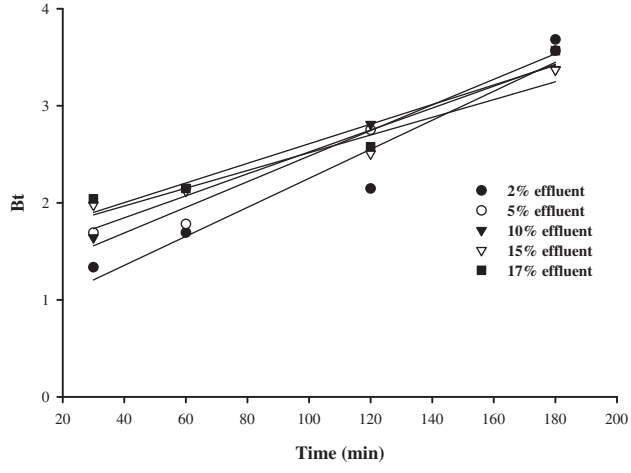

Fig. 7. Boyd plots for effluent adsorption onto *E. nidulans* at different effluent concentrations.

study has shown that this fungus is capable of treating pulp and paper mill effluent [16]. The *A. nidulans* turned dark brown in colour after treatment. The results of isotherm, kinetics and thermodynamics support that adsorption was taking place and after scaling it to bioreactor level it can be used in industries for treating industrial effluent.

4. Conclusions

The isotherm, kinetic and mechanistic studies show that biosorption was involved in decolourization of pulp and paper mill effluent by *E. nidulans*. The optimum pH was 5, temperature was 30˚C, biomass 7.5% and contact time 240 min. The results of this study were well described by Freundlich isotherm and pseudo-second-order kinetic model. Weber–Morris and Boyd plot shows that initially process was governed by boundary layer effect followed by pore diffusion. Mechanism of colour sorption was complex involving both mass transfer and intraparticle diffusion. R_L value indicates that the process was favourable. The values of ΔG°, ΔH_r and E_a show that process was spontaneous, endothermic and dominated by chemical sorption. The results show that this fungus is capable of removing coloured compounds from waste stream and can be used for bioremediation of industrial effluents.

Acknowledgements

Authors thank University Grants Commission, New Delhi, India for providing fellowship. We thank IIT, Delhi and NIPER, Mohali for SEM and FTIR analysis, respectively.

References

[1] A. Singhal, I.S. Thakur, Two step sequential treatment of pulp and paper mill effluent by *Cryptococcus albidus* and *Emericella nidulans* var. nidulans in 2L bioreactor, Can. J. Chem. Eng. 90 (2012) 739–744.
[2] V. Ponnusami, S.N. Srivastava, Studies on application of teak leaf powders for the removal of color from synthetic and industrial effluents, J. Hazard. Mater. 169 (2009) 1159–1162.
[3] R.K. Prasad, S.N. Srivastava, Sorption of distillery spent wash onto fly ash: Kinetics, mechanism, process design and factorial design, J. Hazard. Mater. 161 (2009) 1313–1322.
[4] H. Bolton, Y.A. Gorby, An overview of the bioremediation of metal-contaminated industrial effluents using waste sludges, Water Sci. Technol. 34 (1995) 9–15.
[5] A.H. Sulaymon, D.W. Abbood, A.H. Ali, Competitive biosorption of phenol and lead from synthetic wastewater onto live and dead microorganisms, Desalin. Water Treat. 45 (2012) 331–342.
[6] F. Masood, A. Malik, Biosorption of metal ions from aqueous solution and tannery effluent by *Bacillus* sp. FM1, J. Environ. Sci. Health A Tox. Hazard Subst. Environ. Eng. 46 (2011) 1667–1674.
[7] M. Galun, P. Keller, D. Malki, H. Feldstein, E. Galun, S. Siegel, B. Siegel, Recovery of uranium (VI) from solution using precultured *Penicillium* biomass, Water Air Soil Pollut. 20 (1983) 221–232.
[8] S. Maheswari, A.G. Murugesan, Biosorption of As(III) ions from aqueous solution using dry, heat treated and NaOH treated *Aspergillus nidulans*, Environ. Technol. 32 (2011) 211–219.
[9] S. Srivastava, I.S. Thakur, Biosorption potency of *Aspergillus niger* for removal of chromium (VI), Curr. Microbiol. 53 (2006) 232–237.
[10] Z. Aksu, Determination of the equilibrium, kinetic and thermodynamic parameters of the batch biosorption of nickel(II) ions onto *Chlorella vulgaris*, Process Biochem. 38 (2002) 89–99.
[11] D. Ringot, B. Lerzy, J.-P. Bonhoure, E. Auclair, E. Oriol, Y. Larondelle, Effect of temperature on in vitro ochratoxin A biosorption onto yeast cell wall derivatives, Process Biochem. 40 (2005) 3008–3016.
[12] F. Saiano, M. Ciofalo, S.O. Cacciola, S. Ramirez, Metal ion adsorption by *Phomopsis sp*. biomaterial in laboratory experiments and real wastewater treatments, Water Res. 39 (2005) 2273–2280.
[13] M. Bhanoori, G. Venkateswerlu, In vivo chitin–cadmium complexation in cell wall of *Neurospora crassa*, Biochim. Biophys. Acta, (BBA)—General Subjects 1523 (2000) 21–28.
[14] Y. Pinghe, Y. Qiming, J. Bo, L. Zhao, Biosorption removal of cadmium from aqueous solution by using pretreated fungal biomass cultured from starch wastewater, Water Res. 33 (1999) 1960–1963.
[15] O. Hamdaoui, E. Naffrechoux, Modeling of adsorption isotherms of phenol and chlorophenols onto granular activated carbonPart I. Two-parameter models and equations allowing determination of thermodynamic parameters, J. Hazard. Mater. 147 (2007) 381–394.
[16] A. Singhal, I.S. Thakur, Decolourization and detoxification of pulp and paper mill effluent by *Emericella nidulans* var. nidulans, J. Hazard. Mater. 171 (2009) 619–625.
[17] S.S. Baral, S.N. Das, G.R. Chaudhury, P. Rath, Adsorption of Cr (VI) by treated weed *Salvinia cucullata*: Kinetics and mechanism, Adsorption 14 (2008) 111–121.
[18] B.-E. Wang, Y.-Y. Hu, L. Xie, K. Peng, Biosorption behavior of azo dye by inactive CMC immobilized *Aspergillus fumigatus* beads, Bioresour. Technol. 99 (2008) 794–800.
[19] G.-F. Chen, M.-H. Liu, Adsorption of L-Lysine from aqueous solution using spherical lignin beads: Kinetics and equilibrium studies, Bioresour. Technol. 121 (2012) 298–303.
[20] M. Horsfall Jr., J.L. Vicente, Kinetic study of liquid-phase adsorptive removal of heavy metal ions by almond tree (*Terminalia Catappa*) leaves waste, Bull. Chem. Soc. Ethiop. 21 (2007) 349–362.
[21] G. Bayramoğlu, G. Çelik, M.Y. Arica, Biosorption of Reactive Blue 4 dye by native and treated fungus Phanerocheate chrysosporium: Batch and continuous flow system studies, J. Hazard. Mater. 137 (2006) 1689–1697.

[22] Y.S. Ho, G. McKay, Pseudo-second order model for sorption processes, Process Biochem. 34 (1999) 451–465.
[23] S.S. Baral, S.N. Das, P. Rath, Hexavalent chromium removal from aqueous solution by adsorption on treated sawdust, Biochem. Eng. J. 31 (2006) 216–222.
[24] APHA–AWWA–WEF, 2120 C: Spectrophotometric-Single Wavelength Method in Standard Method for Examination of Water and Wastewater, Washington, DC, 2005.
[25] R.R. Mohammed, M.F. Chong, Treatment and decolorization of biologically treated Palm Oil Mill Effluent (POME) using banana peel as novel biosorbent. J. Environ. Manage. 132 (2014) 237e249.
[26] A.A. Ahmad, B.H. Hameed, Reduction of COD and color of dyeing effluent from a cotton textile mill by adsorption onto bamboo-based activated carbon, J. Hazard. Mater. 172 (2009) 1538–1543.
[27] D. Dionisi, S.S. Bruce, M.J. Barraclough, Effect of pH adjustment, solid–liquid separation and chitosan adsorption on pollutants' removal from pot ale wastewaters, J. Environ. Chem. Eng. 2 (2014) 1929–1936.
[28] M.Y. Arıca, G. Bayramoğlu, Biosorption of Reactive Red-120 dye from aqueous solution by native and modified fungus biomass preparations of *Lentinus sajor-caju*, J. Hazard. Mater. 149 (2007) 499–507.
[29] V.P. Ranjusha, R. Pundir, K. Kumar, M.G. Dastidar, T.R. Sreekrishnan, Biosorption of Remazol Black B dye (Azo dye) by the growing *Aspergillus flavus*, J. Environ. Sci. Health A Tox. Hazard Subst. Environ. Eng. 45 (2010) 1256–1263.
[30] L. Ramrakhiani, R. Majumder, S. Khowala, Removal of hexavalent chromium by heat inactivated fungal biomass of *Termitomyces clypeatus*: Surface characterization and mechanism of biosorption, Chem. Eng. J. 171 (2011) 1060–1068.
[31] G.M. Maciel, C.G. Marques de Souza, C.A. Vaz de Araújo, E. Bona, C. Windson, I. Haminiuk, R. Castoldi, A. Bracht, R.M. Peralta, Biosorption of herbicide picloram from aqueous solutions by live and heat-treated biomasses of *Ganoderma lucidum* (Curtis) P. Karst and *Trametes* sp, Chem. Eng. J. 215–216 (2013) 331–338.
[32] M.X. Loukidou, K.A. Matis, A.I. Zouboulis, M. Liakopoulou-Kyriakidou, Removal of As(V) from wastewaters by chemically modified fungal biomass, Water Res. 37 (2003) 4544–4552.
[33] T. Mathialagan, T. Viraraghavan, Biosorption of pentachlorophenol from aqueous solutions by a fungal biomass, Bioresour. Technol. 100 (2009) 549–558.
[34] A. Singhal, P.K. Jaiswal, I.S. Thakur, Biopulping of bagasse by *Cryptococcus albidus* under partially sterilized conditions, Int. Biodeterior. Biodegrad. 97 (2015) 143–150.
[35] S. Maheswari, A.G. Murugesan, Biosorption of arsenic (III) ion from aqueous solution using *Aspergillus fumigatus* isolated from arsenic contaminated site, Desalin. Water Treat. 11 (2009) 294–301.
[36] B. George, J.I.N. Kumar, R.N. Kumar, P.R. Sajish, Biosorption potentiality of living *Aspergillus niger* Tiegh in removing heavy etal from aqueous solution, Biorem. J. 16 (2012) 195–203.
[37] K. Vijayaraghavan, M.W. Lee, Y.-S. Yun, A new approach to study the decolorization of complex reactive dye bath effluent by biosorption technique, Bioresour. Technol. 99 (2008) 5778–5785.
[38] X.-P. Liao, W. Tang, R.-Q. Zhou, B. Shi, Adsorption of metal anions of vanadium(V) and chromium(VI) on Zr(IV)-impregnated collagen fiber, Adsorption 14 (2008) 55–64.
[39] B.V. Babu, S. Gupta, Adsorption of Cr(VI) using activated neem leaves: Kinetic studies, Adsorption 14 (2008) 85–92.
[40] M.L. Paul, J. Samuel, N. Chandrasekaran, A. Mukherjee, Comparative kinetics, equilibrium, thermodynamic and mechanistic studies on biosorption of hexavalent chromium by live and heat killed biomass of *Acinetobacter junii* VITSUKMW2, an indigenous chromite mine isolate, Chem. Eng. J. 187 (2012) 104–113.
[41] A.H. Sulaymon, D.W. Abbood, A.H. Ali, Competitive biosorption of phenol and lead from synthetic wastewater onto live and dead microorganisms, Desalin. Water Treat. 45 (2012) 331–342.
[42] A.R. Shawwa, D.W. Smith, D.C. Sego, Color and chlorinated organics removal from pulp mills wastewater using activated petroleum coke, Water Res. 35 (2001) 745–749.
[43] S. Chhikara, R. Dhankhar, Biosorption of Cr(VI) ions from electroplating industrial effluent using immobilized *Aspergillus niger* biomass, J. Environ. Biol. 29 (2008) 773–778.
[44] P. Benoit, E. Barriuso, R. Calvet, Biosorption characterization of herbicides, 2,4-D and atrazine, and two chlorophenols on fungal mycelium, Chemosphere 37 (1998) 1271–1282.
[45] Y.S. Ho, J.F. Porter, G. McKay, Equilibrium isotherm studies for the sorption of divalent metal ions onto peat: Copper, nickel and lead single component systems, Water Air Soil Pollut. 141 (2002) 1–33.
[46] M. Hema, S. Arivoli, Rhodamine B adsorption by activated carbon: Kinetics and equilibrium studies, Indian J. Chem. Technol. 16 (2009) 38–45.
[47] D. Wankasi, M. Horsfall Jr., A.I. Spiff, Sorption kinetics of Pb^{2+} and Cu^{2+} ions from aqueous solution by Nipah palm (*Nypa fruticans* Wurmb) shoot biomass, Electron. J. Biotechnol. 9 (2006) 587–592.
[48] T.S. Singh, K.K. Pant, Kinetics and mass transfer studies on the adsorption of Arsenic onto activated alumina and iron oxide impregnated activated alumina, Water Qual. Res. J. Canada 41 (2006) 147–156.
[49] G.S. Gupta, G. Prasad, K.K. Panday, V.N. Singh, Removal of chrome dye from aqueous solutions by fly ash, Water Air Soil Pollut. 37 (1988) 13–24.
[50] S. Özcan, B. Erdem, A. Özcan, Adsorption of Acid Blue 193 from aqueous solutions onto Na–bentonite and DTMA–bentonite, J. Colloid Interface Sci. 280 (2004) 44–54.
[51] Z. Aksu, G. Karabayır, Comparison of biosorption properties of different kinds of fungi for the removal of Gryfalan Black RL metal-complex dye, Bioresour. Technol. 99 (2008) 7730–7741.
[52] V.C. Srivastava, I.D. Mall, I.M. Mishra, Treatment of pulp and paper mill wastewaters with poly aluminium chloride and bagasse fly ash, Colloids Surf., A: Physicochem. Eng. Aspects 260 (2005) 17–28.
[53] A. Jumasiah, T.G. Chuah, J. Gimbon, T.S.Y. Choong, I. Azni, Adsorption of basic dye onto palm kernel shell activated carbon: Sorption equilibrium and kinetics studies, Desalination 186 (2005) 57–64.

Appendix A. Supplementary information and figures

Theoretical background

A.1. Adsorption (equilibrium) isotherms

Four different models were tested [15]. They are as follows:

A.1.1. Langmuir model

The Langmuir model assumes uniform energies of adsorption onto the surface and no transmigration of adsorbate in the plane of the surface. The Langmuir equation may be written as:

$$q_e = q_m K_L C_e/(1 + K_L C_e) \quad \text{(A1)}$$

where q_e is the amount of solute adsorbed per unit weight of adsorbent at equilibrium (mg g^{-1}), C_e the equilibrium concentration of the solute in the bulk solution (mg L^{-1}), q_m is the Langmuir maximum adsorption capacity (mg g^{-1}), and K_L is the constant related to the free energy of adsorption (L mg^{-1}).

The essential characteristics of Langmuir isotherm can be expressed in terms of dimensionless constant separator factor or equilibrium parameters R_L, given by:

$$R_L = 1/(1 + K_L C_0) \quad \text{(A2)}$$

The parameter R_L indicated the shape of the isotherm ($R_L > 1$ isotherm is unfavorable, $R_L = 1$ it is linear, $0 < R_L < 1$ it is favorable and $R_L = 0$ it is irreversible) [3].

A.1.2. Freundlich model

The Freundlich equation can be written as:

$$q_e = K_F C_e^{1/n} \quad \text{(A3)}$$

where q_e is the amount of solute adsorbed per unit weight of adsorbent at equilibrium (mg g^{-1}), K_F is a constant indicative of the relative adsorption capacity of the adsorbent ($mg^{1-(1/n)}$ $L^{1/n}$ g^{-1}) and n is a constant indicative of the intensity of the adsorption. The Freundlich expression is an exponential equation and therefore, assumes that as the adsorbate concentration increases, the concentration of adsorbate on the adsorbent surface also increases.

A.1.3. Elovich model

The equation defining the Elovich model is based on a kinetic principle assuming that the adsorption sites increase exponentially with adsorption, which implies a multilayer adsorption. It is expressed by the relation:

$$q_e/q_m = K_E C_e \exp(-q_e/q_m) \quad \text{(A4)}$$

where q_e is the amount of solute adsorbed per unit weight of adsorbent at equilibrium (mg g^{-1}), K_E is the Elovich equilibrium constant (L mg^{-1}) and q_m is the Elovich maximum adsorption capacity (mg g^{-1}). If the adsorption obeys Elovich equation, Elovich maximum adsorption capacity and Elovich constant can be calculated from the slopes and the intercepts of the plot ln (q_e/C_e) vs. q_e.

A.1.4. Temkin model

The derivation of the Temkin isotherm assumes that the fall in the heat of sorption is linear rather than logarithmic, as implied in the Freundlich equation. The Temkin isotherm has generally been applied in the following form [45]:

$$q_e = (RT/\Delta Q) \ln K_T C_e \quad \text{(A5)}$$

$$q_e = (RT/\Delta Q) \ln K_T + (RT/\Delta Q) \ln C_e \quad \text{(A6)}$$

where q_e is the amount of solute adsorbed per unit weight of adsorbent at equilibrium (mg g^{-1}), K_T is Temkin constant, R is universal gas constant (8.314 JK^{-1} mol^{-1}), T is temperature in Kelvin (303 for this study), C_e the equilibrium concentration of the solute in the bulk solution (mg L^{-1}).

A.2. Adsorption kinetic models

Adsorption data were applied to two kinetic models i.e. pseudo-first-order and pseudo-second-order.

A.2.1. Pseudo-first-order kinetic model

Pseudo-first-order kinetic model (also called Lagergren model) was calculated for different effluent concentrations ranging from 2 to 17% using equation [52]:

$$\ln (q_e - q_t) = \ln q_e - (k_f/2.303)t \quad \text{(A7)}$$

where q_e is the amount of solute adsorbed per unit weight of adsorbent at equilibrium (mg g^{-1}), q_t (mg g^{-1}) is the amount of solute adsorbed per unit weight of adsorbent at time t (min), k_f is rate constant of pseudo-first-order kinetic model (min^{-1}). Plot is drawn between ln ($q_e - q_t$) vs. t.

A.2.2. Pseudo-second-order kinetic model

Pseudo-second-order kinetic model was calculated using equation [52]:

$$d_{qt}/d_t = k_s (q_e - q_t)^2 \quad \text{(A8)}$$

where q_e is the amount of solute adsorbed per unit weight of adsorbent at equilibrium (mg g^{-1}), q_t (mg g^{-1}) is the amount of solute adsorbed per unit weight of adsorbent at time t (min), k_s is rate constant of pseudo-second-order

kinetic model (g/mg min). Integrating the above equation for boundary conditions $q_t = 0$ at $t = 0$ and $q_t = q_t$ at any time t.

$$t/q_t = 1/k_s q_e^2 + (1/q_e)t \tag{A9}$$

$k_s q_e^2$ is Ho constant (h_o) defined as initial sorption rate (mg/g min) at time = 0. Plot was draw in between t/q_t vs. t.

A.3. Validation of models (Error functions)

Various error functions used to evaluate the isotherm and kinetic models are given below [15,53].

A.3.1. APE: average percentage error

The experimental values of q_e^{exp} and C_e were initially treated with linearized equations of Freundlich, Langmuir and Elovich to determine the model parameters. After determining the best model the values of q_e^{calc} were recalculated using non-linear equations for isotherms and linear equations for kinetic models. The reconstitute isotherms/kinetic models were compared with initial isotherms/kinetic models to evaluate the error in the models. Linear correlation coefficients (r^2) showed the fit between experimental data and linearized forms of isotherm equations, while the error functions indicated the fit between the experimental (q_e^{exp}) and calculated (q_e^{calc}) values of adsorption capacity used for plotting isotherm/kinetic curves.

$$\text{APE } (\%) = \sum_{i=1}^{p} \left[\left(q_e^{Exp} - q_e^{Calc} / q_e^{Exp} \right) / N \right] \times 100 \tag{A10}$$

where N is the number of experimental data.

A.3.2. The sum of the squares of the errors (SSE)

The equation for Sum of the Squares of the Errors (SSE) is as follows:

$$\text{SSE} = \sum_{i=1}^{p} \left(q_e^{Exp} - q_e^{Calc} \right)_i^2 \tag{A11}$$

A.3.3. A composite fractional error function (HYBRID)

The equation for Composite Fractional Error Function (HYBRID) is as follows:

$$\text{HYBRID} = \sum_{i=1}^{p} \left[\left(q_e^{Exp} - q_e^{Calc} \right)^2 / q_e^{Exp} \right]_i \tag{A12}$$

A.3.4 Chi square Error Function (χ^2)

The equation for Chi square Error Function (χ^2) is as follows:

$$\chi^2 = \sum_{i=1}^{p} \left(q_e^{Exp} - q_e^{Calc} \right)^2 / q_e^{Calc} \tag{A13}$$

A.3.5. Marquardt's per cent standard deviation (MPSD)

The equation for Marquardt's Per cent Standard Deviation (MPSD) is as follows:

$$\text{MPSD} = \sum_{i=1}^{p} \left(q_e^{Exp} - q_e^{Calc} / q_e^{Exp} \right)_i^2 \tag{A14}$$

A.3.6. Average relative error (ARE)

The equation for ARE is as follows:

$$\text{ARE} = \sum_{i=1}^{p} \left| q_e^{Exp} - q_e^{Calc} / q_e^{Exp} \right|_i \tag{A15}$$

A.3.7. The sum of the absolute errors (EABS)

The equation for Sum of the Absolute Errors (EABS) is as follows:

$$\text{EABS} = \sum_{i=1}^{p} \left| q_e^{Exp} - q_e^{Calc} \right|_i \tag{A16}$$

A.4. Pore and film diffusion models

Two different models intraparticle diffusion plot (Weber–Morris plot) and Boyd plot were evaluated [18,19]. They are as follows:

The equation for Weber–Morris intraparticle relation is given by:

$$q_t = K_i t^{0.5} + I \tag{A17}$$

where q_t (mg/g) is adsorbent capacity at time t, K_i (g/mg $min^{0.5}$) is intraparticle diffusion coefficient, t is time and I (mg/g) is intercept.

The Boyd kinetic expression is given by:

$$B_t = 0.4977 - \ln(1 - F) \quad \text{(A18)}$$

$$F = q_t/q_o \quad \text{(A19)}$$

where B_t is mathematical function of F at time t, q_t (mg/g) is adsorbent capacity at time t and q_o (mg/g) is adsorbent capacity at infinite time.

2.5. Thermodynamics

A.5.1. Activation energy (E_a)

Activation energy (E_a) was calculated using rate constant of pseudo second order kinetic model (k_s) and Ho constant (h_o) by linear form of Arrhenius expression [20,21]. The equation is:

$$\ln k_s = \ln h_o - E_a/RT \quad \text{(A20)}$$

where k_s (g/mg min) is pseudo-second-order rate constant, h_o (mg/g. min) is Ho constant (pre-exponential factor), E_a (kJ mol^{-1}) is activation energy, R (8.314 J/mol K) is gas constant and T is temperature in Kelvin [22]. Ho constant was calculated by the equation given below:

$$h_o = k_s q_e^2 \quad \text{(A21)}$$

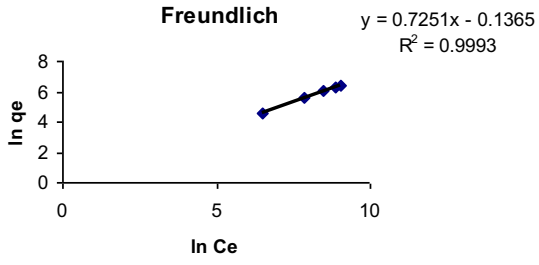

Fig. B1. Freundlich isotherm plot for adsorption of effluent onto *E. nidulans*.

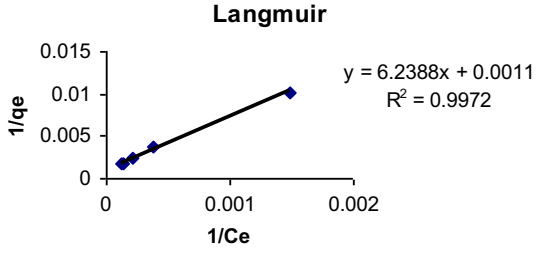

Fig. B2. Langmuir isotherm plot for adsorption of effluent onto *E. nidulans*.

where h_o (mg/g min) is Ho constant (pre-exponential factor), k_s (g/mg min) is pseudo-second-order rate constant and q_e is adsorbent capacity at equilibrium (mg/g).

A.5.2. Gibbs energy change (ΔG°)

Gibbs free energy of adsorption (ΔG°) can be related to Langmuir constant (K_L) using equation:

$$(\Delta G^\circ) = -RT \ln K_L \quad \text{(A22)}$$

where ΔG° (kJ mol^{-1}) is Gibbs free energy, R (8.314 J/mol. K) is gas constant, T is temperature in Kelvin and K_L (L mg^{-1}) is Langmuir constant [2].

A.5.3. Isosteric heat of adsorption (ΔH_r)

Isosteric heat of adsorption (ΔH_r) was calculated using the equation:

$$(\Delta H_r) = [R \ln(C_2/C_1)]/(1/T_2) - (1/T_1) \quad \text{(A23)}$$

where ΔH_r (kJ mol^{-1}) is Isosteric heat of adsorption. C_2 and C_1 are the concentration of sorbate (mg/L) in the solution at temperature T_2 and T_1 (K), respectively. R (8.314 J/mol K) is gas constant [23].

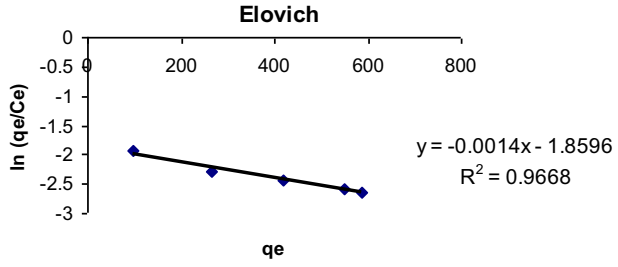

Fig. B3. Elovich isotherm plot for adsorption of effluent onto *E. nidulans*.

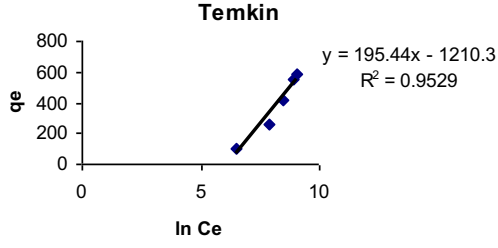

Fig. B4. Temkin isotherm plot for adsorption of effluent onto *E. nidulans*.

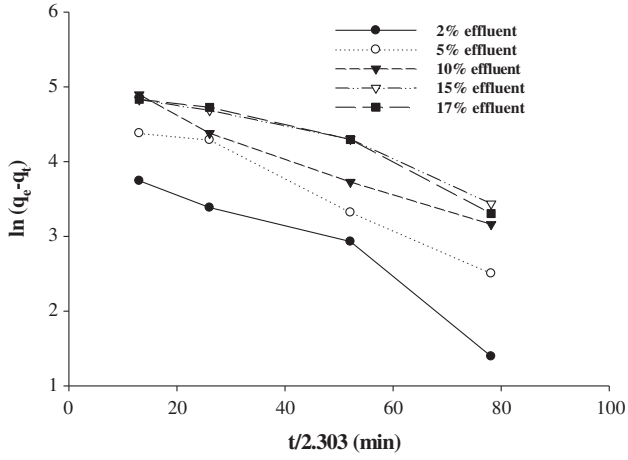

Fig. B5. Pseudo-first-order plots for adsorption of effluent onto *E. nudulans* at different effluent concentrations.

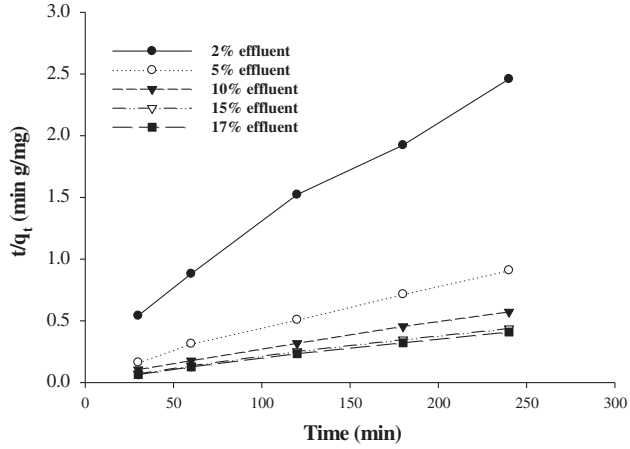

Fig. B6. Pseudo-second-order plots for adsorption of effluent onto *E. nudulans* at different effluent concentrations.